JOURNAL OF SYNCHROTRON RADIATION

ISSN 1600-5775

# *In situ* N *K*-edge XANES study of iron, cobalt and nickel nitride thin films

Nidhi Pandey,[a] Mukul Gupta,[a]* D. M. Phase[a] and Ajay Gupta[b]

[a]UGC-DAE Consortium for Scientific Research, University Campus, Khandwa Road, Indore 452 001, India, and [b]Department of Physics, University of Petroleum and Energy Studies, Dehradun 248 007, India.
*Correspondence e-mail: mgupta@csr.res.in

Received 13 January 2021
Accepted 30 June 2021

Edited by S. M. Heald, Argonne National Laboratory, USA

**Keywords:** soft X-ray absorption spectroscopy; *in situ* studies; N *K*-edge XANES; transition metal nitrides; reactive sputtering; X-ray absorption spectroscopy; 3*d* transition metal nitride thin films.

A prototype *in situ* X-ray absorption near-edge structure (XANES) system was developed to explore its sensitivity for ultra-thin films of iron-nitride (Fe-N), cobalt-nitride (Co-N) and nickel-nitride (Ni-N). They were grown using DC-magnetron sputtering in the presence of an $N_2$ plasma atmosphere at the experimental station of the soft XAS beamline BL01 (Indus-2, RRCAT, India). XANES measurements were performed at the N *K*-edge in all three cases. It was found that the N *K*-edge spectral shape and intensity are greatly affected by increasing thickness and appear to be highly sensitive, especially in low-thickness regions. From a certain thickness of ∼1000 Å, however, samples exhibit a bulk-like behavior. On the basis of the obtained results, different growth stages were identified. Furthermore, the presence of a molecular $N_2$ component in the ultra-thin regime (<100 Å) was also obtained in all three cases studied in this work. In essence, this prototype *in situ* system reveals that N *K*-edge XANES is a powerful technique for studying ultra-thin films, and the development of a dedicated *in situ* system can be effective in probing several phenomena that remain hitherto unexplored in such types of transition metal nitride thin films.

## 1. Introduction

X-ray absorption spectroscopy (XAS) is a powerful tool for detecting the electronic structure, local geometry and bonding environment of materials (De Groot, 2001; Henderson *et al.*, 2014). XAS can be broadly subdivided as X-ray absorption near-edge structure (XANES) and X-ray absorption fine structure (EXAFS). The tunability of synchrotron radiation allows XAS measurements to be performed using hard (energy $E > 5$ keV) or soft X-rays ($E < 3$ keV), and therefore XAS can be termed as hard XAS (HXAS) or soft XAS (SXAS) (Baker *et al.*, 2017; Shadike *et al.*, 2018). Metal *K*-edges XAS typically utilizes HXAS to excite 1*s* electrons. SXAS covers the *L*-edges of various metals as well as the *K*-edge of ligands (lighter elements) such as Na, C, N, S and O. Both *K*- and *L*-edges can be used to examine the unoccupied 3*d* states of transition metals (Baker *et al.*, 2017; Shadike *et al.*, 2018).

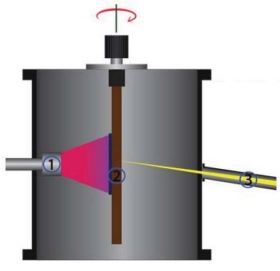

Such absorption transitions lead to specific sensitivities and provide complimentary information. The metal *K*-edge is sensitive to coordination number and symmetry due to the ligand-enabled mixing of the 4*p* metal character into the metal 3*d* orbitals and therefore can be used to quantify the mixing of 3*d*–4*p* as well as the covalency of ligand–metal bonds; whereas metal *L*-edge XAS enables $2p \rightarrow 3d$ transitions, which are a more direct probe for covalent delocalization (Baker *et al.*, 2017). Thus, SXAS is highly sensitive to the unoccupied electronic states near the Fermi level, which provides the

formal valence, the chemical potential and the orbital character of the metal and ligands. Moreover, it is sensitive to the spin state, fraction of metal 3*d* orbitals hybridized with ligand-2*p* and also enables the separation of donor bonding and back bonding, *etc*. (Shadike *et al.*, 2018; Wang *et al.*, 2015). In addition, the analysis of the HXAS suffers from poor energy resolution at the metal *K*-edge (>1 eV for 3*d* metals) due to the short lifetime of the 1*s* core hole. On the other hand, SXAS has a better resolution (<0.5 eV for 3*d* metals) (Baker *et al.*, 2017; Shadike *et al.*, 2018).

XAS measurements are typically performed in three different ways: (i) transmission mode, (ii) fluorescence (FY) mode and (iii) total electron yield (TEY) mode. For soft X-rays, absorption is quite large, and therefore in transmission mode the samples have to be extremely thin to penetrate. This issue is solved by detecting the XAS signal in FY and TEY modes. However, even the FY mode suffers from (i) 'self-absorption' effects and (ii) multiplet effects due to the dependence of the final state on fluorescence decay. Therefore, XAS in FY is not pure. In addition, the TEY detection is based on a simple drain-current set-up. Therefore, the application of TEY mode is indispensable in obtaining reliable XAS data in the soft X-ray region (Tamenori, 2013).

SXAS measurements typically require a high-vacuum chamber due to the short attenuation length of such photons in air. These measurements can be either performed *ex situ* or *in situ*. Here, the term *ex situ* refers to measurements of a sample prepared elsewhere and brought on-site for measurements whereas *in situ* XAS indicates preparation of a sample within the measurement system without exposure to the atmosphere. As the probe depth in the TEY mode is typically 5–10 nm, it becomes a highly surface-sensitive technique. Also, since contamination due to exposure of a sample to the atmosphere can easily penetrate well beyond this probe depth, absorption spectra from *ex situ* SXAS measurements may have some ambiguity. Therefore, *in situ* SXAS are advantageous as information from a cleaner surface can be obtained. In addition, the possibility to perform such measurements *in situ* or *in operando* can provide real-time investigation of physical and chemical properties (Shadike *et al.*, 2018; Chang *et al.*, 2020; Aksoy *et al.*, 2010).

For example, *in situ* XAS measurements have been successfully demonstrated to investigate the real-time local geometric and electronic structure information of 2D electrode materials during the charging/discharging process (Shadike *et al.*, 2018; Chang *et al.*, 2020). In the case of thin films, *in situ* SXAS was also conducted at metal *L*-edges with the evolution of film thickness. Variations in branching ratio, FWHM, spin–orbit coupling and spin state with growing thickness in Cr (Aksoy *et al.*, 2010), Fe and Ni films (Akgul *et al.*, 2014) have been studied. Aksoy *et al.* (2010) reported that after a critical thickness (above 80 Å) the Cr thin film shows a layer-by-layer type growth mode. The variation in the electronic structure with the evolution of Cr film thickness was studied in detail using *in situ* SXAS measurements and it was found that the thinner Cr films exhibit an atomic-like structure with island growth which progressively became a more bulk-like structure with film thickness (Aksoy *et al.*, 2010). A similar study on Fe and Ni films was also performed using *in situ* SXAS at metal *L*-edges (Akgul *et al.*, 2014). Detailed analysis of Fe and Ni *L*-edges with increasing thicknesses revealed that the electronic structure is significantly different for films having a thickness below 60 Å (Akgul *et al.*, 2014). In another report by Esaka *et al.* (1997), the oxidation mechanisms of TiN and CrN thin films were investigated by *in situ* SXAS measurements at the N *K*-edge.

Thus the *in situ* synchrotron XAS characterization method has been demonstrated to be a powerful tool to investigate the real-time local geometric and electronic structural information of electrode materials during the charge/discharge process and with the evolution of film thickness. In view of this, *in situ* XAS investigations on iron nitride (Fe-N), cobalt nitride (Co-N) and nickel nitride (Ni-N) thin films are presented and discussed in this work.

## 2. Experimental details

A magnetron sputtering system was added at the experimental station of the soft XAS beamline BL01 at Indus 2, RRCAT, Indore, India (Phase *et al.*, 2014). Thin films of magnetic nitrides were deposited and characterized by N *K*-edge absorption measurements immediately after (not during) the deposition without exposing them to air. This arrangement is referred to as *in situ* XAS. A schematic diagram of the *in situ* XAS system is shown in Fig. 1. As can be seen, the synchrotron radiation (SR) beam hits directly the vertically mounted sample holder. The *in situ* XAS chamber was separated from the beamline by a UHV gate valve (not shown). A magnetron source (1 inch diameter; Angstrom Sciences, USA) was placed directly facing the SR beam (size 0.2 mm × 2 mm) and in between them the sample holder was mounted on a rotary motion feedthrough. The center of the SR beam and that of the magnetron source were matched so that the signal from the most homogeneous part of the film could be obtained. The magnetron source was mounted with a Wilson seal arrange-

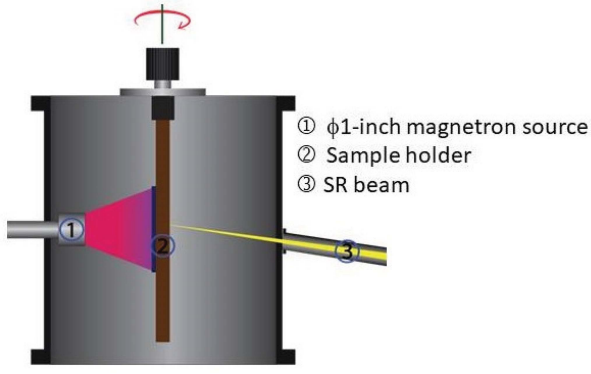


**Figure 1**
Schematic diagram of the *in situ* XAS system used for deposition of Fe-N, Co-N and Ni-N thin films from a 1 inch-diameter magnetron source and N *K*-edge XANES measurements at the soft X-ray absorption spectroscopy beamline BL01, Indus-2.

ment so that the distance between the magnetron source and the sample could be optimized. The magnetron source was equipped with a shutter so that the target could be pre-sputtered prior to deposition of the actual sample. Several test deposition sequences were followed to calibrate the thickness of the film at a fixed power. It was found that the thickness of the film varies linearly with deposition time, as expected within a DC-magnetron sputtering process.

Some photographs of the experimental chamber and various key components like magnetron source, sample holder, mass flow controller *etc.* can be seen in Fig. 2. The deposition chamber of capacity ∼25 l was pumped with a 300 l $s^{-1}$ turbomolecular pump. Elemental targets of Fe, Co or Ni with a purity of 99.995% (thickness 0.5 mm) were used for sputtering in a pure $N_2$ plasma atmosphere. The $N_2$ gas (purity 99.9995%) flow was fixed at about 20 sccm (sccm = standard cubic cm $min^{-1}$). The base pressure was $2 \times 10^{-8}$ mbar and the pressure during thin film deposition was about $5 \times 10^{-3}$ mbar due to the flow of $N_2$ gas.

Before carrying out the *in situ* XAS experiment, the target was pre-sputtered to remove surface contaminations on the target itself. The sputtering power used was about 15 W (450 V, DC) and the target–substrate distance was about 5 cm. All samples were deposited at ambient temperature without any intentional heating on clean substrates. After each deposition the chamber was evacuated back to UHV conditions and N *K*-edge XANES measurements were carried out in TEY mode. The number of scans was averaged to improve the data reliability and statistics. The energy resolution of the beamline under these conditions was about 0.2 eV. Prior to the *in situ* XAS measurements, a few test samples of Fe-N, Co-N and Ni-N were deposited (on Si and $SiO_2$ substrates) under the same conditions discussed above to determine their deposition rates and crystalline structures. These test samples were then employed for X-ray reflectivity and X-ray diffraction measurements (using Bruker D8 Advance with Cu *Kα* X-rays) to obtain the deposition rates and structural information, respectively. From our earlier studies, it was found that reactive sputtering with nitrogen alone results in the formation of FeN (Gupta *et al.*, 2019), CoN (Gupta *et al.*, 2020) and $Ni_2N$ (Pandey *et al.*, 2021) phases.

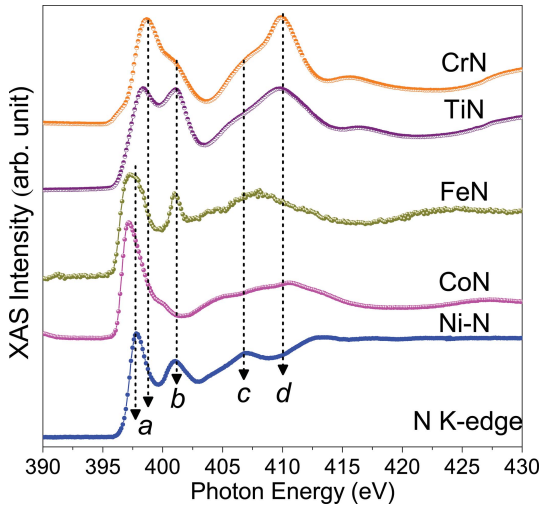


**Figure 3**
N *K*-edge absorption spectra of bulk-like (∼1500 Å) late transition metal nitrides (Fe-N, Co-N, Ni-N) are compared with early ones (TiN, CrN). Prominent features marked as *a*–*d* can be seen in each case. N *K*-edge spectra of CrN and TiN have been taken from Behera *et al.* (2020).

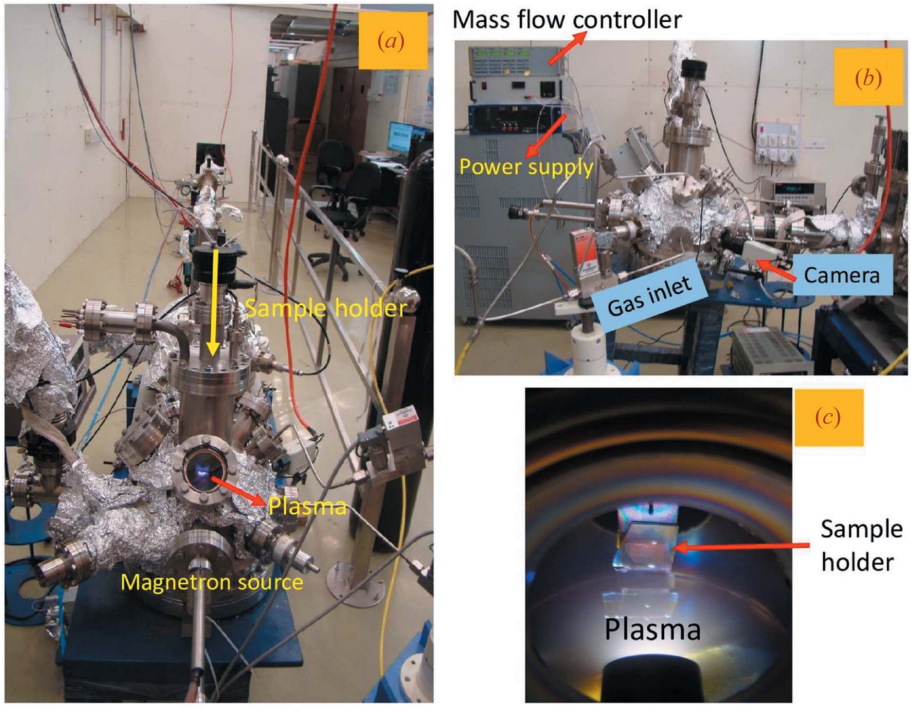


**Figure 2**
Photographs of the *in situ* XAS system showing the entire experimental station along the incoming beam (*a*), side view of the experiential station (*b*) and inside view of the magnetron source and sample holder during deposition (*c*).

N *K*-edge XANES of bulk-like (∼1500 Å thick) Fe-N, Co-N and Ni-N thin film samples are shown in Fig. 3. They are compared with the rather well studied TiN (Esaka *et al.*, 1997) and CrN (Tripathi *et al.*, 2019) samples. As can be seen from the figure, N *K*-edge XANES of CrN and TiN films shows four prominent features at 398.5, 400, 406.5 and 409.8 eV, labeled *a*, *b*, *c* and *d*, respectively. Here features *a* and *b* correspond to electronic transitions to the unoccupied hybridized states of N 2*p* and metal 3*d* orbitals. Features *c* and *d* are assigned to the unoccupied N 2*p* states hybridized to metal 4*sp* orbitals. Similarly, in the case of Fe-N, Co-N and Ni-N thin films, features *a*, *b*, *c* and *d* correspond to the same electronic transitions as seen for TiN and CrN films. However, it should be noted here that the feature *a* is slightly shifted to lower energies in Fe-N, Co-N and Ni-N films compared with TiN and CrN,

indicating that in the former cases N is in the nearly $3^-$ state. Using the assignment of these features, the *in situ* N *K*-edge XANES can also be understood.

## 3. Results

### 3.1. *In situ* XANES study of Fe-N thin films

N *K*-edge XANES spectra measured *in situ* for Fe-N films of thicknesses between 2 and 2500 Å are shown in Fig. 4(*a*). In order to compare the intensity of the XANES spectral features, pre- and post-edge normalizations were performed using *Athena* software (Ravel & Newville, 2005). We can see that the spectra gradually change with increasing thickness.

Even in the sample with lowest thickness (2 Å), two dominant features at 401.6 eV, with FWHM about 0.75 eV, and 407.7 eV can be seen with some additional features at the lower as well as at the higher energy side. The spectral peak obtained at 401 eV has also been previously observed in several nanocrystalline/amorphous transition metal nitride thin films (Chen, 1997; Ruck *et al.*, 2004*a*,*b*; Granville *et al.*, 2005). This peak at 401 eV has been reported to be responsible for the $\pi^*$ resonance of molecular nitrogen ($N_2$) trapped within the films (Chen, 1997; Ruck *et al.*, 2004*a*,*b*; Granville *et al.*, 2005). In a review article by Chen (Chen, 1997), the peak at 401.6 eV was attributed to the excitation from the N 1*s* to the $2\pi_g$ level [the lowest unfilled (antibonding) $N_2$ molecular orbital] and assigned as $\pi^*$ resonance, while the feature at about 407.7 eV is due to $\sigma^*$ resonance. In the present case, the similarity in peak position and FWHM therefore allows us to characterize the 401 eV peak as the $\pi^*$ resonance of molecular nitrogen.

However, on slightly increasing the thickness to about 4 Å, the XANES spectra change significantly. Along with the sharp peak at 401.6 eV (assigned as *b*), another feature on the lower energy side at 397.4 eV (assigned as *a*) started to appear. In addition, the $\sigma^*$ resonance is also modified , now assigned as *c* and *d*, shown in Fig. 4(*a*). The position of feature *a* matches well with previously reported TiN and CrN films (Chen, 1997; Esaka *et al.*, 1997; Tripathi *et al.*, 2019) and corresponds to feature *a* shown and discussed in Fig. 3. Thereby, feature *a* can be assigned to unoccupied hybridized states of N 2*p* and Fe 3*d* orbitals while for *c* and *d* the features (at about 406.1 and 409.8 eV) may correspond to unoccupied N 2*p* states hybridized to Fe 4*sp* orbitals in Fe-N film. Note that the features *c* and *d* change significantly after 40 Å; however, after 80 Å they remain almost the same until the end of the deposition. Moreover, it is also to be noted here that in the higher thickness range (above 1000 Å) the N *K*-edge spectra match well with the previously reported Fe-N phase with zinc blend (ZB) type structure (Niti *et al.*, 2020). The spectral shape and intensity of all features change with thickness, suggesting that the electronic structure of Fe-N changes with increasing thickness.

To gain further insight into this, an enlarged view of features *a* and *b* of N *K*-edge spectra is shown in Fig. 4(*b*). From here, we can see that the positions of features *a* and *b* remain almost unchanged up to a thickness of 80 Å; however, the intensity of *b* decreases gradually with thickness, and vice versa for *a*. At the next thickness of 150 Å, the change in the spectral shape and energy position of *a* and *b* indicates that the surface chemistry is modified. Furthermore, after 150 Å, an abrupt shift in features *a* and *b* to the high energy side can be clearly

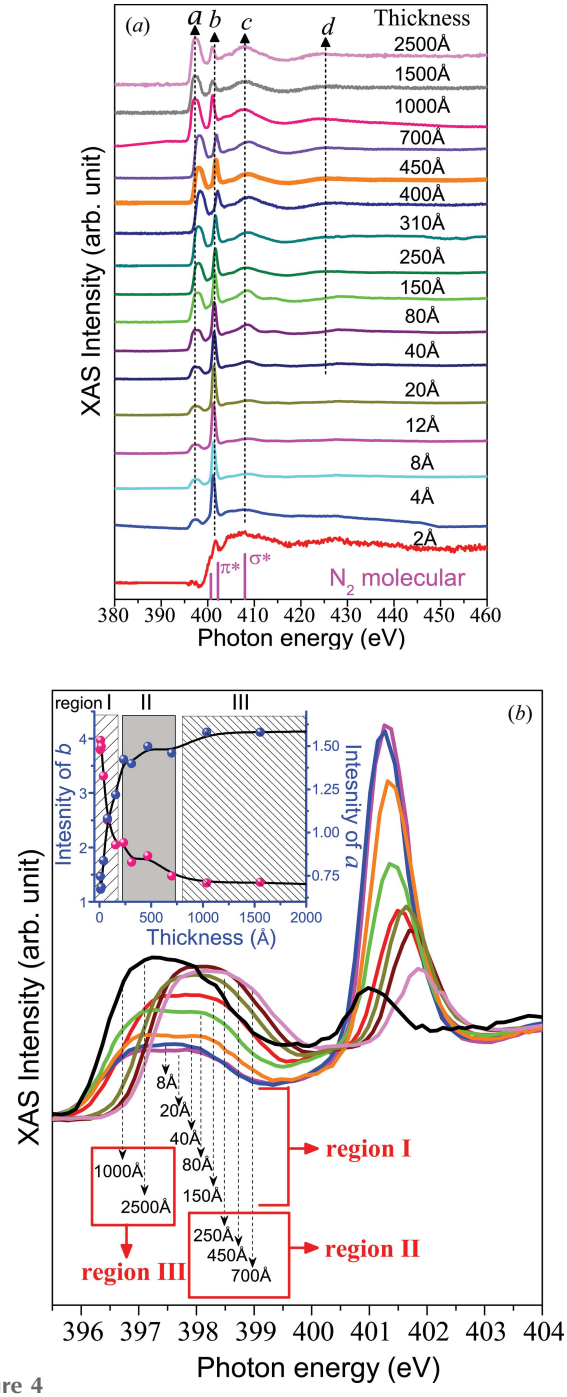


**Figure 4**
(*a*) N *K*-edge XANES spectra measured in TEY mode taken *in situ* during the growth of Fe-N film on a quartz substrate at 300 K using reactive magnetron sputtering. (*b*) Enlarged region covering features *a* and *b*. The inset shows the variation in the intensity of features *a* and *b* with thickness. The different regions I, II and III are classified on the basis of changes in the energy position and intensity variation of features *a* and *b* with increasing thickness.

seen and remains almost the same in the thickness range 250–700 Å, indicating that the surface electronic states do not change considerably in this region. On further increasing the thickness to 1000–2500 Å, features *a* and *b* shift back to the low energy side.

In addition, the intensity of features *a* and *b* also changes with increasing thickness, which can be seen from the inset of Fig. 4(*b*). The intensity of feature *b* decreases, while *a* increases rapidly with increasing thickness followed by a deceleration after 700 Å. However, above 1000 Å the intensity variation becomes almost constant, and the spectra also match well with bulk FeNe (Niti *et al.*, 2020). The energy shift of features *a* and *b* also varies in a similar trend with thickness, and in such a way the Fe-N film growth regions can be classified as I, II and III, as shown in the inset of Fig. 4(*b*) and discussed in Section 4.

### 3.2. *In situ* XANES study of Co-N thin films

*In situ* N *K*-edge XANES spectra taken during deposition of Co-N thin films are shown in Fig. 5. In the thinnest sample (1 Å) the molecular $N_2$ like features can be clearly seen with $\pi^*$ resonance (marked as *b* in Fig. 5) at 400.4 eV. Beyond this (>1 Å), the feature *b* splits into two features (marked as *b* and *b*′ in Fig. 5). As the thickness increases to 4 Å, another feature begins to appear at about 397.5 eV at the onset of feature *b*, marked as *a*. Here again, the obtained features *a*, *c* and *d* are similar to the features in Fig. 3.

Note that another feature appears at 389.8 eV that corresponds to the second-order Co $L_3$-edge (shown in Fig. 5) and, therefore, the second-order $L_2$-edge will appear at 396.7 eV, which seems to be merging with feature *a*, since the second-order intensity of $L_2$ should always be lower than $L_3$ but here the $L_2$ region becomes more prominent than $L_3$. This clearly suggests overlapping of the N *K*-edge edge features into the $L_2$ second order. With increasing thickness, the feature *a* becomes quite pronounced, signifying that the hybridization between the Co 3*d* and N 2*p* states increases with increasing thickness.

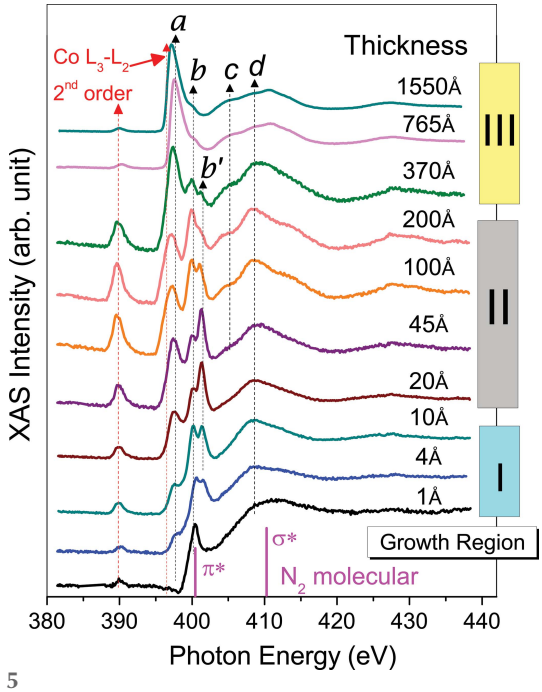


**Figure 5**
N *K*-edge XANES spectra measured in TEY mode taken *in situ* during the growth of Co-N film on a quartz substrate at 300 K using reactive magnetron sputtering. The different growth regions are also shown.

On increasing the thickness from 4 to 10 Å, the N *K*-edge XANES spectra remain almost constant, whereas the spectral shape is modified by increasing the thickness to 20 Å and remains almost the same up to 200 Å. However, for thickness $\geq$370 Å, again a noticeable variation in the spectral shape can be seen. From here, it can also be seen that the intensity of *a* becomes highest and the features *b* and *b*′ appear to merge. For thickness >200 Å, it appears that the molecular $N_2$ features become insignificant. Therefore, such variations show that, above 200 Å, feature *b* corresponds to the electronic transition to hybridized states of N 2*p* and Co 3*d*, not to the molecular $N_2$.

Based on the above results, the growth process can be classified into three different stages (shown in Fig. 5), similar to Fe-N. The molecular $N_2$ component appears to be prominently present in region I with another Co-N phase up to a thickness of 10 Å. Whereas in region II (up to 200 Å) the contribution of molecular $N_2$ appears to be low, while the other phase component increases. In region III (above 370 Å), the $N_2$ features become negligible and only the contribution from the Co-N phase can be seen.

### 3.3. *In situ* XANES study of Ni-N thin films

*In situ* N *K*-edge XANES spectra of Ni-N thin films are shown in Fig. 6. Similar to Fe-N and Co-N, in the ultrathin region (1 Å) the $\pi^*$ feature (marked as *b* in Fig. 6) at 401.4 eV corresponding to molecular $N_2$ can be seen. On increasing the thickness to 4 Å, another feature (marked by *a*) starts to emerge around 397.7 eV. Similar to the case shown in Fig. 3, it stems from the transition of the N 2*p* and Ni 3*d* states to hybridized states. Here, also, the spectral shape changes significantly, as the thickness increases to 10 Å, and remains nearly the same up to 100 Å. In this thickness range of 10–100 Å, feature *b* further splits into *b* and *b*′, and feature *a* is also enhanced which may signify even greater hybridization between the Ni 3*d* and N 2*p* states.

In addition, it is also interesting to note that a pre-edge feature can also be seen in the thickness range 10–200 Å. It is maximum at 100 Å, reducing significantly at 200 Å, and vanishing completely afterwards. As the intensity of the pre-edge directly relates the coordination geometry around the probing atom, the presence of the pre-edge here can be directly related to a transformation into a more non-centrosymmetric environment. On further increasing the thickness to 200 Å, the spectra change drastically and maintain nearly the same spectral shape up to the highest thickness of 2000 Å. In this thickness range 200 to 2000 Å, the intensity and FWHM of feature *a* increase considerably. For thicknesses >100 Å, we find that the molecular $N_2$ features become insignificant, while feature *a* becomes dominant with

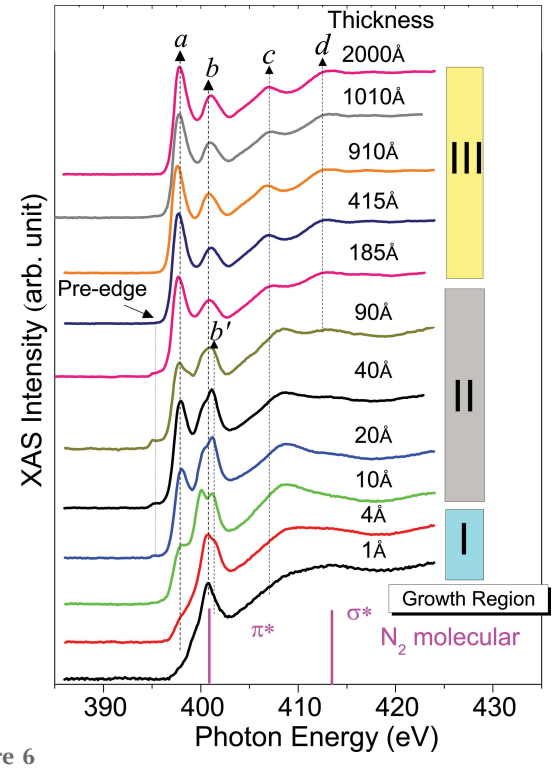


**Figure 6**
N *K*-edge XANES spectra measured in TEY mode taken *in situ* during the growth of Ni-N film on a quartz substrate at 300 K using reactive magnetron sputtering. The different growth regions are also shown.

increasing thickness. Moreover, features *c* and *d* correspond to the higher-energy 4*sp* states, as found for the Fe-N and Co-N films.

Similar to the Fe-N and Co-N films discussed above, in the Ni-N films the growth process is also observed in three different stages (shown as regions I, II and III in Fig. 6). Region I (up to 4 Å) has a molecular $N_2$ component along with another minor Ni-N phase. Region II, ranging from 10 to 100 Å, may be related to the mixture of molecular $N_2$ with increased contribution from the Ni-N phase. In region III (200–2000 Å), the surface chemistry is again modified and shows the absence of any molecular $N_2$ component.

## 4. Discussion

As described above, the N *K*-edge spectra of bulk-like Fe-N film (thickness >1000 Å) matches very well with ZB-type Fe-N film (Niti *et al.*, 2020). In several reports it has been emphasized that the Fe-N phase is formed when Fe is sputtered in a pure $N_2$ plasma atmosphere (Niti *et al.*, 2020; Gupta *et al.*, 2019, 2011; Tayal *et al.*, 2015). Therefore, the formation of the Fe-N phase can also be expected in the present work as the deposition was performed under similar conditions. The strong dependence of the N *K*-edge spectra on thickness indicates that different growth stages [shown as region I, II and III in Fig. 4(*b*)] take place during the deposition of Fe-N thin film. Region I appears to consist of a molecular $N_2$ component with a minor ZB phase. Even in this region the surface electronic structure changes to a large extent even with slightly increasing film thickness and appears to be quite sensitive to thickness. Region II is dominated by the ZB structure. In region II, the surface coordination changes from region I, however, maintain an almost similar behavior throughout this region. The hybridization between Fe and N is again modified from region II to region III. Region III may only have ZB-type coordination because it matches well with the previously described N *K*-edge spectra for ZB-type FeN (Niti *et al.*, 2020). Similarly, in the cases of the Co-N and Ni-N thin films growth processes, we found that the surface chemistry is greatly modified with increasing thickness and seems to be highly sensitive in the low thickness region, specifically in the ultra-thin regime below 100 Å. Different growth regions have also been assigned in the case of the *in situ* growth processes of Co-N and Ni-N. However, based on the above results, it can be seen that above 1000 Å thickness a bulk-like structure is obtained in all cases, where the variation in the spectral shape becomes almost constant.

An interesting outcome is also reflected in terms of the observation of the molecular $N_2$ component in the ultra-thin region in all three cases. The presence of molecular $N_2$ can be related to some pernitride phases as previously reported for nitrogen-rich iron, cobalt and nickel pernitride phases (Wessel & Dronskowski, 2011; Wu *et al.*, 2018; Laniel *et al.*, 2018; Bykov *et al.*, 2018; Niwa *et al.*, 2017, 2019). However, detailed polarization-dependent XAS measurements will be needed to strongly claim the presence of molecular $N_2$ or related phases in the ultra-thin region. Nevertheless, such results allow us to point out that, irrespective of the magnetic 3*d* transition metal nitride, the molecular $N_2$ related phase seems to be a common phenomenon.

## 5. Conclusions

In this work, we demonstrated a prototype system for performing *in situ* XAS measurements at the soft XAS beamline BL-01, Indus 2, India. This method was effectively utilized to grow and investigate Fe-, Co- and Ni-nitride thin films using *in situ* N *K*-edge XANES measurements, even within sub-monolayer thicknesses. It was found that the spectral shape of the N *K*-edge absorption spectra exhibit a strong dependence on the thickness of the films. These changes take place in different thickness regions. For ultra-thin films (<100 Å), an $N_2$ molecular component was prominent but it disappears gradually as the thickness increases beyond 100–150 Å. Thus, our *in situ* N *K*-edge absorption measurements provide subtle and important information about the structural behavior with thickness variation of metal nitride thin films.

## Acknowledgements

We would like to thank Rakesh Sah for the help provided during the development and *in situ* XANES measurements, to Layanta Behera for preparing the schematic diagrams of the beamline and *in situ* systems. We are thankful to A. K. Sinha, V. Ganesan and A. Banerjee for support and encouragement.

## Funding information

Funding for this research was provided by: UGC-DAE CSR; DST New Delhi.

## References

Akgul, G., Akgul, F. A. & Ufuktepe, Y. (2014). *Vacuum*, **99**, 211–215.
Aksoy, F., Akgül, G., Ufuktepe, Y. & Nordlund, D. (2010). *J. Alloys Compd.* **508**, 233–237.
Baker, M. L., Mara, M. W., Yan, J. J., Hodgson, K. O., Hedman, B. & Solomon, E. I. (2017). *Coord. Chem. Rev.* **345**, 182–208.
Behera, L., Pandey, N. & Gupta, M. (2020). *AIP Conf. Proc.* **2265**, 030310.
Bykov, M., Bykova, E., Aprilis, G., Glazyrin, K., Koemets, E., Chuvashova, I., Kupenko, I., McCammon, C., Mezouar, M., Prakapenka, V., Liermann, H.-P., Tasnádi, F., Ponomareva, A. V., Abrikosov, I. A., Dubrovinskaia, N. & Dubrovinsky, L. (2018). *Nat. Commun.* **9**, 2756.
Chang, Y.-M., Lin, H.-W., Li, L.-J. & Chen, H.-Y. (2020). *Mater. Today Adv.* **6**, 100054.
Chen, J. G. (1997). *Surf. Sci. Rep.* **30**, 1–152.
Esaka, F., Furuya, K., Shimada, H., Imamura, M., Matsubayashi, N., Sato, H., Nishijima, A., Kawana, A., Ichimura, H. & Kikuchi, T. (1997). *J. Vac. Sci. Technol. A*, **15**, 2521–2528.
Granville, S., Ruck, B., Budde, F., Koo, A., Downes, J. E., Trodahl, H., Bittar, A., Strickland, N., Williams, G., Lambrecht, W., Learmonth, T., Smith, K. E., Kennedy, V. J., Markwitz, A. & Schmitt, T. (2005). *Phys. Rev. B*, **72**, 205127.
Groot, F. de (2001). *Chem. Rev.* **101**, 1779–1808.
Gupta, M., Kumar, Y., Tayal, A., Pandey, N., Caliebe, W. & Stahn, J. (2020). *SN Appl. Sci.* **2**, 41.
Gupta, M., Pandey, N., Niti, Reddy, V. R., Phase, D. M., Schlage, K., Wille, H. & Gupta, A. (2019). *Hyperfine Interact.* **240**, 99.
Gupta, M., Tayal, A., Gupta, A., Reddy, V., Horisberger, M. & Stahn, J. (2011). *J. Alloys Compd.* **509**, 8283–8288.
Henderson, G. S., de Groot, F. M. & Moulton, B. J. (2014). *Rev. Mineral. Geochem.* **78**, 75–138.
Laniel, D., Dewaele, A. & Garbarino, G. (2018). *Inorg. Chem.* **57**, 6245–6251.
Niti, Gupta, M., Rajput, P., Jha, S. N. & Gupta, A. (2020). *J. Phys. Chem. Solids*, **147**, 109653.
Niwa, K., Fukui, R., Terabe, T., Kawada, T., Kato, D., Sasaki, T., Soda, K. & Hasegawa, M. (2019). *Eur. J. Inorg. Chem.* **2019**, 3753–3757.
Niwa, K., Terabe, T., Kato, D., Takayama, S., Kato, M., Soda, K. & Hasegawa, M. (2017). *Inorg. Chem.* **56**, 6410–6418.
Pandey, N., Gupta, M. & Stahn, J. (2021). *J. Alloys Compd.* **851**, 156299.
Phase, D. M., Gupta, M., Potdar, S., Behera, L., Sah, R. & Gupta, A. (2014). *AIP Conf. Proc.* **1591**, 685–686.
Ravel, B. & Newville, M. (2005). *J. Synchrotron Rad.* **12**, 537–541.
Ruck, B. J., Koo, A., Lanke, U. D., Budde, F., Granville, S., Trodahl, H. J., Bittar, A., Metson, J. B., Kennedy, V. J. & Markwitz, A. (2004*b*). *Phys. Rev. B*, **70**, 235202.
Ruck, B. J., Koo, A., Lanke, U. D., Budde, F., Trodahl, H. J., Williams, G. V. M., Bittar, A., Metson, J. B., Nodwell, E., Tiedje, T., Zimina, A. & Eisebitt, S. (2004*a*). *J. Appl. Phys.* **96**, 3571–3573.
Shadike, Z., Zhao, E., Zhou, Y.-N., Yu, X., Yang, Y., Hu, E., Bak, S., Gu, L. & Yang, X.-Q. (2018). *Adv. Energy Mater.* **8**, 1702588.
Tamenori, Y. (2013). *J. Synchrotron Rad.* **20**, 419–425.
Tayal, A., Gupta, M., Gupta, A., Rajput, P. & Stahn, J. (2015). *Phys. Rev. B*, **92**, 054109.
Tripathi, Y., Gupta, R., Seema, Gupta, M., Phase, D. & Rajput, P. (2019). *Thin Solid Films*, **670**, 113–121.
Wang, L., Song, J., Qiao, R., Wray, L. A., Hossain, M. A., Chuang, Y.-D., Yang, W., Lu, Y., Evans, D., Lee, J.-J., Vail, S., Zhao, X., Nishijima, M., Kakimoto, S. & Goodenough, J. B. (2015). *J. Am. Chem. Soc.* **137**, 2548–2554.
Wessel, M. & Dronskowski, R. (2011). *Chem. Eur. J.* **17**, 2598–2603.
Wu, L., Tian, R., Wan, B., Liu, H., Gong, N., Chen, P., Shen, T., Yao, Y., Gou, H. & Gao, F. (2018). *Chem. Mater.* **30**, 8476–8485.